View Article Online
DOI: 10.1039/D1TB01972D

ARTICLE

Carbon nanotubes-reinforced cell-derived matrix-silk fibroin hierarchical scaffolds for bone tissue engineering applications

Received 00th January 20xx,
Accepted 00th January 20xx

DOI: 10.1039/x0xx00000x

Rafael Lemos [a, b, c], F. Raquel Maia [a, b,†], Viviana P. Ribeiro [a, b], João B. Costa [a, b], Paulo J. G. Coutinho [c], Rui L. Reis [a, b], and Joaquim M. Oliveira [a, b]

In bone tissue engineering, the development of advanced biomimetic scaffolds has led to the quest for biomotifs in scaffold design that better recreate bone matrix structure and composition and hierarchy at different length scales. In this study, an advanced hierarchical scaffold consisting of silk fibroin combined with decellularized cell-derived extracellular matrix and reinforced with carbon nanotubes was developed. The goal of the carbon nanotubes-reinforced cell-derived matrix-silk fibroin hierarchical scaffolds is to harvest the individual properties of its constituents to introduce hierarchical capacity in order to improve standard silk fibroin scaffolds. The scaffolds were fabricated using enzymatic cross-linking, freeze modeling, and decellularization methods. The developed scaffolds were assessed for pore structure and mechanical properties showing satisfying results to be used in bone regeneration. The developed carbon nanotubes-reinforced cell-derived matrix-silk fibroin hierarchical scaffolds showed to be bioactive in vitro and expressed no hemolytic effect. Furthermore, cellular in vitro studies on human adipose-derived stem cells (hASCs) showed that scaffolds supported cell proliferation. The hASCs seeded onto these scaffolds evidenced similar metabolic activity to standard silk fibroin scaffolds but increased ALP activity. The histological stainings showed cells infiltration into the scaffolds and visible collagen production. The expression of several osteogenic markers was investigated, further supporting the osteogenic potential of the developed carbon nanotubes-reinforced cell-derived matrix-silk fibroin hierarchical scaffolds. The hemolytic assay demonstrated the hemocompatibility of the hierarchical scaffolds. Overall, the carbon nanotubes-reinforced cell-derived matrix-silk fibroin hierarchical scaffolds presented the required architecture for bone tissue engineering applications.

[a] 3B's Research Group, I3B's – Research Institute on Biomaterials, Biodegradables and Biomimetics, University of Minho, Headquarters of the European Institute of Excellence on Tissue Engineering and Regenerative Medicine, AvePark, Parque de Ciência e Tecnologia, Zona Industrial da Gandra, 4805-017 Barco, Guimarães, Portugal;
[b] ICVS/3B's - PT Government Associated Laboratory, Braga/Guimarães, Portugal;
[c] Centre of Physics (CFUM), University of Minho, Campus de Gualtar, 4710-057 Braga, Portugal.

† Corresponding author: F. Raquel Maia (raquel.maia@i3bs.uminho.pt).

Introduction

The increasing rate of musculoskeletal pathologies affects the world population due to ever-higher life expectancy and aging. Since bone-related diseases dramatically affect functional and patient quality of life, it is important to develop improved treatment strategies that promote bone tissue regeneration.(1) Bone tissue engineering solutions based on advanced scaffolds are a promising strategy and alternative to

View Article Online
DOI: 10.1039/D1TB01972D

conventional approaches that use autografts, which are considered the current gold standard for clinical practices.[2] In this reasoning, developing advanced biomimetic scaffolds mimicking the natural bone tissue in its complex three-dimensional (3D) structure and composition is a step forward in biomaterial research and more patient-specific therapeutics.[3,4] Several fabrication techniques have been explored for engineering hierarchical scaffolds with tuned structure [5], mechanical properties, and biochemical composition.[6] The type of biomaterial also plays an important role in designing a hierarchical scaffold and ultimately will dictate the success or failure of tissue regeneration.[7] Silk fibroin is a natural-based biopolymer whose porosity can be controlled through ice-templating, allowing the display of anisotropic or hierarchical structures.[8] Furthermore, it can possess synergistic and advantageous features for bone tissue engineering scaffolding applications.[9] Silk fibroin is a widely used material in bone tissue engineering due to its versatility and interesting natural properties.[10–12] Nonetheless, its main disadvantage is its poor mechanical strength for bone tissue engineering applications.[13] A solution to overcome this problem relies on the use of carbon nanotubes, which have successfully improved the mechanical properties of scaffolds systems.[14,15] Introducing important biochemical factors via nanoparticle delivery is a widely used approach for hierarchical scaffolds.[6,16] Although effective, it is often a one-dimensional approach unable to emulate the complex composition of the bone and its extracellular matrix. The use of decellularized matrices of the native tissue is of great promise to address this issue since its biochemical composition provides optimal biological cues.[17,18]

In this study, we aim to develop silk fibroin hierarchical scaffolds combining silk fibroin, carbon nanotubes, and decellularized cell-derived extracellular matrix for bone tissue engineering applications. The carbon nanotubes-reinforced cell-derived matrix-silk fibroin hierarchical scaffolds were produced using enzymatic cross-linking, freeze templating, and decellularization methods. In *in vitro* studies, human adipose-derived stem cells were cultured in an osteogenic culture medium in order to obtain a cell-derived extracellular matrix with osteogenic properties. Different scaffold formulations were tested according to their mechanical, structural, and biological properties. Overall, in this study, a promising approach towards 3D hierarchical scaffolds was developed for potential applications in bone tissue engineering.

Materials and methods

Scaffold's production and characterization

Silk fibroin solution production

Silk derived from the silkworm *Bombyx mori* in the form of cocoons was provided by the Portuguese Association of Parents and Friends of Mentally Disabled Citizens (APPACDM, Castelo Branco, Portugal). Sericin protein was removed from the cocoons using a 0.02 M boiling sodium carbonate (Sigma Aldrich, USA) solution for 1 h, followed by a 30 min wash with boiling distilled water to remove the degumming solution altogether, obtaining pure silk fibroin (SF). Next, the SF was dissolved using a 9.3 M lithium bromide (Sigma Aldrich, USA) solution for 1 h at 70°C. The resulting solution was then submitted to dialysis in distilled water for 48 h, with regular water changes, using the benzoylated dialysis tubing (MWCO: 2 kDa) (Sigma Aldrich, USA). SF was concentrated using a 20 wt% poly (ethylene glycol) (Sigma Aldrich, USA) solution for a minimum of 6 h. A small amount of SF solution was transferred to an Eppendorf and placed at 70°C overnight to obtain the dry weight and calculate the SF solution's final concentration. The resulting SF solution was stored at 4°C until further use.

Cell-derived ECM production

The human adipose-derived stem cells (hASCs) were obtained from the isolation of lipoaspirate samples gathered under a protocol previously established with the Department of Plastic Surgery of Hospital da Prelada (Porto, Portugal). All subjects were informed and gave their consent. Next, 3,000 cells per cm2 were seeded into a 150 cm2 T-flask in α-MEM medium (Gibco, USA) supplemented with 10% fetal bovine serum (FBS) (Gibco, USA) and 1% antibiotic/antimycotic (AB) (Gibco, USA), and kept at 37°C in a humidified atmosphere of 5% v/v CO2 in air. Medium changes were performed every 4 days until cells reached 80% of confluence. Afterward, hASCs were sub-cultured at an initial cell density of 3,000 cells per cm2 in a 150 cm2 T-flask and kept under α-MEM medium supplemented with 0.05 mM ascorbic acid (FUJIFILM Wako Pure Chemical Corporation, USA), 10 mM β-Glycerophosphate (Sigma Aldrich, USA), 100 nM dexamethasone (Sigma Aldrich, USA), 10% FBS and 1% AB. Cells were cultured for 6 weeks under a humidified atmosphere of 5% v/v CO2 in air, and the medium was changed twice a week in order to produce a condensed cell monolayer with high amounts of ECM.

Decellularization

The decellularization was performed as described in Maia et al.[19] Briefly, previously obtained condensed cell monolayers were subjected to six cycles of freezing at -80°C for 12 h followed by thawing at 37°C until thoroughly defrosted. Afterward, packed cell monolayers were cut into smaller pieces with ≈ 3 mm. Then, they were incubated in a solution of 2% (v/v) Triton X-100 (Sigma Aldrich, USA) with 10% (v/v) AB for 24 h, at 4°C under 200 rpm. To remove Triton X-100 solution, monolayers were centrifuged at 5,000 rpm for 5 min at 4°C, and the supernatant was discarded. The condensed cell monolayers were vortexed and incubated in 0.1% (w/v) of SDS (Sigma Aldrich, USA) with 10% (v/v) AB for 48 h at 4°C under 200 rpm.

View Article Online DOI: 10.1039/D5TB01375D

Condensed cell monolayers were centrifuged at 5,000 rpm for 5 min at 4°C, and the supernatant was discarded. Again, the structures were vortexed. To remove any trace of detergents, the monolayers were transferred to ultrapure water and sonicated for 45 min on ice. The ultrapure water was removed by centrifugation at 5,000 rpm at 4°C for 5 min, the supernatant was discarded, and the monolayers vortexed. Condensed cell monolayers were subjected to the action of 0.006% of DNase (Thermo Scientific, USA) with 10% AB for 96 h at 4°C and under 200 rpm. Lastly, the DNase solution was removed by centrifugation at 5,000 rpm at 4°C for 5 min, and the supernatant was discarded. The resulted decellularized cell-derived matrix (dCDM) was then frozen and lyophilized for 48 h.

Evaluation of decellularization effectiveness

The decellularization effectiveness was assessed through visualization of cell nuclei and matrix preservation by histologic analysis and DNA quantification. The decellularized tissue was transferred to histological cassettes and fixed with 10% (v/v) formalin solution (Thermo Scientific, USA). After paraffin embedding (Microm EC350-1, Thermo Scientific, USA), samples were processed in a spin tissue processer (Microm STP 120, Thermo Scientific, USA) and sectioned with 10 µm thickness by a microtome (Spencer 820, American Optical Company, USA). Standard hematoxylin and eosin (HE; Thermo Scientific, USA) staining was performed to assess the presence of cell nuclei, and Masson's trichrome (Bio-Optica staining kit, Italy) was performed to evaluate the preservation of collagen content. DNA extraction was achieved using the DNeasy Blood & Tissue Kit (Qiagen, Germany) according to the manufacturer's instructions. Similarly, the DNA quantification was performed using Quant-IT PicoGreen dsDNA Assay Kit 2000 assays (Thermo Scientific, USA) following the manufacturer's instructions. A microplate reader (Synergy HT, Bio-Tek, USA) was used to read the fluorescence intensity at 485/20 nm (excitation) and 530/20 nm (emission). The results were converted into ng/ml through a standard curve produced with standard dsDNA solutions at increasing concentrations, ranging from 250 ng/ml to 2,000 ng/ml. Finally, the dsDNA quantification values were normalized by the dCDM dry weight.

dCDM solution preparation

The dCDM was dissolved using 1 ml of 0.01 M hydrochloric acid (Honeywell, USA) and 10 mg pepsin (Fisher Scientific, USA) per mg of dCDM. The dCDM was placed in the solution under agitation at 200 rpm at room temperature for 72 h until it was fully dissolved. After this step, the pH level was adjusted to 7.0 with sodium hydroxide.

Scaffold fabrication

For scaffold fabrication, four different conditions were prepared, SF scaffolds (SF scaffolds), SF combined with multi-walled carbon nanotubes scaffolds (Sigma-Aldrich) (SF/CNT scaffolds), SF combined with dCDM scaffolds (SF/dCDM scaffolds), and SF combined with dCDM and CNT (SF/dCDM/CNT scaffolds). For SF scaffolds, horseradish peroxidase (HRP) (type VI, 0.84 mg/ml) (Sigma Aldrich, USA) and hydrogen peroxide solution (H_2O_2, 0.36 wt%; Panreac, Spain) were added to an 8 wt% SF solution that was diluted with distilled water. This mixture was then incubated at 37°C for 30 min. To obtain SF/dCDM scaffolds, SF solution was combined with dCDM solution for a final concentration of 8 wt% SF and 1 mg/ml of dCDM. For the SF/CNT scaffolds, SF was combined with CNT to an end concentration of 8 wt% SF and 1 mg/ml of CNT. The SF/dCDM/CNT were fabricated combining SF, dCDM, and CNT to an end concentration of 8 wt% of SF, 1 mg/ml of dCDM, and 1 mg/ml of CNT. All scaffolds, SF/dCDM, SF/CNT, and SF/dCDM/CNT, were fabricated as described to develop SF scaffolds. In this reasoning, each solution was combined with HRP (type VI, 0.84 mg/ml) and hydrogen peroxide solution. This mixture was then incubated at 37°C for 30 min. After the enzymatic cross-linking, the scaffolds were frozen at - 80°C for 2 h and then freeze-dried for 24 h.

Micro-computed tomography (Micro-CT)

The microarchitecture of the produced scaffolds was analyzed with a high-resolution micro-CT SkyScan 1272 scanner (Bruker, USA) with a pixel size of 10 µm. Standardized cone-beam reconstruction software (NRecon v1.4.3, SkyScan) was used for data sets reconstructions. Binary images with a dynamic threshold of 22–40 (gray values) were obtained through segmentation of the sample's representative data set. Then, the obtained results were used for morphometric analysis (CT Analyser, v1.5.1.5, SkyScan) and construction of 3D models (CTVox, v2.4, SkyScan). After 3D reconstruction, different thresholds were applied to analyze the various components of the scaffolds.

Dynamic mechanical analysis (DMA)

The viscoelastic measurements were investigated using a DMA 8000 (PerkinElmer, USA) in the compressive setting. The scaffolds (n=3) were immersed in phosphate buffer saline (PBS, Sigma-Aldrich) overnight at 37°C. The geometry of the scaffolds was measured (with a micrometer of precision), clamped in the DMA apparatus, and immersed in a PBS bath with the temperature set to 37°C. After equilibration at 37°C, the DMA spectra were acquired through a frequency scan ranging from 0.1 to 10 Hz. A constant strain amplitude of 50 µm was applied in each experiment.

Bioactivity test

The *in vitro* bioactivity evaluation was performed as described elsewhere.[20] Briefly, scaffolds were soaked for 7 and 14 days in conical tubes containing simulated body fluid solution (SBF). The SBF solution was prepared under continuous

View Article Online
DOI: 10.1039/D1TB01972D

agitation of 60 rpm and at 37°C with the following ion concentrations: Na^+ 142.0 mM, K^+ 5.0 mM, Ca^{2+} 2.5 mM, Mg^{2+} 1.5 mM, Cl^- 148.8 mM, HPO^{4-} 1.0 mM, HCO_3^{2-} 4.2 mM, and SO_4^{2-} 0.5 mM (20). Then the pH was corrected to 7.4, a value similar to the human blood plasma's pH. After, the scaffolds were rinsed with distilled water and dried at 37°C overnight. Then, the scaffolds were analyzed using SEM (JEOL, JSM-6010LV) and elemental chemical analysis by energy-dispersive X-ray spectroscopy (EDS).

Cellular in vitro studies

Cell seeding

All scaffolds were sterilized with oxide ethylene before cell seeding. Previously isolated hASCs were cultured at a density of 3,000 cells per cm2 into a 150 cm2 T-flask in α-MEM medium supplemented with 10% FBS and 1% AB and maintained at 37°C under a humidified atmosphere of 5% v/v CO2 in air. Medium changes were performed every 4 days until cells reached 80% of confluence. At this point, cells were detached and seeded at the scaffolds. For that, a drop (30 µl) of 150,000 hASCs in the medium was seeded on top of SF, SF/dCDM, SF/CNT, and SF/dCDM/CNT scaffolds. After 1 h at 37°C, the drop was entirely absorbed by the scaffolds, and 1ml of α-MEM medium with 10% FBS and 1% AB was added to each well. Cultures were maintained in 48 non-adherent well plates in order to minimize cell adhesion to the bottom of the plates. Cultures were kept at 37°C in a humidified atmosphere of 5% (v/v) CO2 in air.

Metabolic activity

Metabolic activity was evaluated after 1, 14, and 21 days making use of 20% (v/v) of Alamar Blue reagent (ALAMAR BLUE®, AbD, UK) in α-MEM culture medium, constructs were covered to protect from the light and incubated for 3 h at 37°C with 5% CO_2 under a humidified atmosphere of 5% (v/v). Then, into a new 96-well cell culture plate, 100 µl per well of supernatant were pipetted in triplicate. A microplate reader (Synergy HT, Bio-Tek, USA) was used to read the fluorescence intensity at 530/20 nm (excitation) and 590/35 nm (emission). Alamar Blue in medium served as blank. Values were normalized with DNA values for each time point.

DNA content

DNA content was evaluated after 1, 14, and 21 days of culture. Scaffolds were rinsed with PBS followed by adding 1 ml of ultra-pure water into each well and incubating at 37°C for 1 h. Scaffolds were then stored at −20°C until analysis. Before DNA quantification, the constructs were placed in an ultrasound bath for 30 min at 37°C to ensure cell lysis. Quant-IT PicoGreen dsDNA Assay Kit was employed following the manufacturer's specifications to quantify dsDNA from cell lysates. A microplate reader was used to read the fluorescence intensity at 485/20 nm (excitation) and 530/20 nm (emission), and the results were converted through a standard curve obtained with standard dsDNA solutions at increasing concentrations, ranging from 250 ng/ml to 2,000 ng/ml.

Histology staining

Samples were collected after 1, 14, and 21 days and processed for histology. In this sense, constructs were transferred to histological cassettes and fixed with 10% (v/v) formalin solution. After paraffin embedding, samples were processed in a spin tissue processer and sectioned with 10 µm thickness using a microtome. Standard hematoxylin and eosin staining was performed using an automatic stainer (Microm HMS 7740, Thermo Scientific, USA) to assess cell distribution and collagen deposition by Masson's trichrome.

Scanning Electron Microscopy

Scanning electron microscopy (SEM, JSM-6010 LV, JEOL, Japan) was used to analyze the microarchitecture of the scaffolds and observe the cell morphology after the seeding. For SEM analysis, the scaffolds were sliced into halves, and the inner surface of the scaffolds was observed. Scaffolds were fixated in formalin 10% and, before analysis, sputter-coated with gold using a Leica EM ACE600 coater (Leica Microsystems, Austria). For the cell-seeded scaffolds, these were fixated in formalin 10% and rehydrated with a series of ethanol concentrations (30, 50, 70, 90, and 10% v/v), twice each concentration for 15 min. Lastly, the scaffolds were placed in hexamethyldisilazane and left overnight at room temperature (RT) to dry. Before analysis, the scaffolds were sputter-coated with gold.

Alkaline phosphatase activity quantification

To quantify ALP activity, cell lysate previously produced was used. Thus, 80 µl of cell lysate were combined with 20 µl of 1.5 M of Alkaline buffer solution (Sigma-Aldrich) and 100 µl of 4 mg/ml of phosphatase substrate (Sigma-Aldrich, USA). Then samples were incubated protected from light for 1 h at 37°C. Reaching this stage, the reaction was halted by adding 100 µl of 0.3 M of NaOH (Panreac AppliChem), and a microplate reader (Synergy H, Bio-Tek, USA) was used to read the absorbance at 405 nm. The ALP activity per h was determined using a standard curve obtained from different dilutions of 4-Nitrophenol (Sigma-Aldrich, USA) solution 10 mM, ranging from 0 to 250 µM and normalized by the dsDNA quantification values.

RNA Isolation and Real-Time Quantitative Reverse Transcriptase-Polymerase Chain Reaction (qRT-PCR)

The total mRNA from the seeded scaffolds was extracted using the Direct-zolTM RNA MiniPrep kit (Zymo Research, USA),

View Article Online
DOI: 10.1039/D1TB01072D

following the manufacturer's instructions. Briefly, after 14 and 21 days of culture, the constructs were washed with PBS solution, immersed in 300 µl of TRI Reagent, and stored at −80°C until further use. Samples were thawed at room temperature and sonicated using an ultrasonic processor (Sonics Materials VCX-130PB Ultrasonic Processor, USA) to lyse the cells completely. RNA quantification and purity were evaluated through NanoDrop ND-1000 spectrophotometer (Nano-Drop Technologies, USA). Complementary DNA (cDNA) synthesis was performed following the protocol from the qScriptTM cDNA synthesis Kit (Quanta Biosciences, USA) using a MiniOpticon real-time PCR detection system (BioRad, USA). To obtain single-stranded cDNA through qScript Reverse Transcriptase (RT), 100 ng of total RNA was used. The cDNA was further used as a template for the amplification of osteogenic genes (ALP, Runx-2, Col Iα, and OPN) (Table 1) using the PerfeCTa SYBR Green FastMix kit (Quanta Biosciences, USA) according to the manufacturer's instructions. Forty-five cycles of denaturation (95°C, 10 s), annealing (temperature specific for each gene, 25 s), and extension (72°C, 30 s) were carried out in a Mastercycler ep realplex real-time PCR system (Eppendorf, Germany). The transcript expression data of each sample were normalized to the housekeeping gene glyceraldehyde-3-phosphate-dehydrogenase (GAPDH) of that sample for each tested time point. The relative gene expression quantification was calculated as calibrator the expression levels of hASCs collected at the time of cell seeding (day 0), according to the Livak ($2-\Delta\Delta Ct$) method.

Gene	*Sequences*		T_m (°C)
	Forward (5'-3')	**Reverse (5'-3')**	
GAPDH	ACAGTCAGCCGCATCTTCTT	GACAAGCTTCCCGTTCTCAG	58.4
Col Iα	CGAAGACATCCCACCAATCAC	GTCACAGATCACGTCATCCGC	59.6
ALP	CTCCTCGGAAGACACTCTG	AGACTGCGCCTGGTAGTTG	60
OPN	CCCACAGACCCTTCCAAGTA	GGGGACAACTGGAGTGAAAA	58.4
Runx-2	TTCAGACCAGCAGCACTC	CAGCGTCAACACCATCATTC	58.1

Table 1 - Primer list for osteogenic-related markers.

Cell viability and morphology

The cell viability was assessed by calcein-AM and propidium iodide (PI) (Life Technologies, Carlsbad, CA, USA) staining. At each time point, seeded scaffolds were incubated in 1 µg/ml calcein-AM and 5 µg/ml PI prepared in the cultured medium for 30 min in the dark at 37°C in 5% CO_2 under a humidified atmosphere of 5% (v/v). Then, samples were immediately analyzed by confocal microscopy (Leica TCS SP8).

The cell morphology was assessed by F-actin staining. First, cells were rinsed with PBS, fixed with 10% Neutral Buffered Formalin (ThermoFisher Scientific) for 20 min and permeabilized for 5 min with 0.1% v/v Triton X-100 (Sigma-Aldrich) in PBS. Afterwards, F-actin filaments were stained with Phalloidin–Tetramethylrhodamine B isothiocyanate (Sigma-Aldrich, 1:100) and nuclei were counterstained with 1:1000 of the stock of 4,6-Diamidino-2-phenyindole, dilactate solution (DAPI, 1mg/mL, Biotium). Samples were analysed by confocal microscopy (Leica TCS SP8).

Hemolytic assay

To assess the hemolytic activity levels of developed scaffolds, 5 ml of blood were mixed with 45 ml of PBS. Then, to obtain the red blood cells, samples were centrifuged (1,000× g, 4°C) for 10 min, and the supernatant was discarded. The centrifugation step was repeated until obtaining clear PBS solution, thus indicating that the pellet was clean. Afterward, the obtained pellet was measured and was combined with PBS to make a solution of 3% (w/V). At this point, 80 µl of the previous solution was transferred to a well of a 96-well plate, and each developed scaffold was placed inside the solution. As positive control (i.e., 100% red blood cell lysis), 80 µl of Triton X-100 was added to the solution, while as negative control (i.e., 0% red blood cell lysis), 80 µl of PBS was added. The plates were incubated at 37°C for 4 h and afterward centrifuged at 1,000 × g for 10 min and 4°C. Finally, the supernatant (80 µl) of each well was pipetted into a new 96-well plate, and the absorbance was measured at 558 nm. For each sample, three wells were prepared, and data were normalized with the controls, using the following equation 1:

$$\text{Hemolysis (\%)} = [(Abs_{sample} - Abs_{PBS})/(Abs_{Triton\ X\text{-}100} - Abs_{PBS})] \times 100 \quad \text{Eq. 1}$$

Statistical analysis

Statistical analyses were carried out using GraphPad Prism 6.07. First, the Shapiro-Wilk test was performed to assess data normality. Non-parametric Mann-Whitney test was used to determine the differences in the PCR results. The non-parametric tests, the Kruskal-Wallis test followed by Dunn's test, were used to analyze the ALP expression results, metabolic activity, and cell proliferation. The critical value of statistical significance was $p<0.05$. Data are cited as mean ± standard deviation.

Results

Various characterization and biological assays were performed to assess the viability and cytocompatibility of the developed scaffolds. The hASCs were cultured onto the four scaffold formulations: SF, SF/dCDM, SF/CNT, and SF/dCDM/CNT scaffolds, where SF scaffolds were used as control.

Scaffolds characterization

View Article Online
DOI: 10.1039/D1TB01972D

Evaluation of decellularization effectiveness

Hematoxylin-eosin and Masson's Trichrome staining were performed on the decellularized condensed monolayers to verify the presence of nuclei and collagen, respectively, to confirm successful decellularization. As it can be observed from Figure 1, nuclei were successfully removed from dCDM, while collagen was maintained as compared with control (CTRL), i.e., no decellularized matrices. Furthermore, the efficiency of the decellularization process was confirmed through dsDNA quantification analysis. Results show that the value of DNA was inferior to 50 ng/mg of dCDM dry weight, the accepted threshold for effective decellularization.[21]

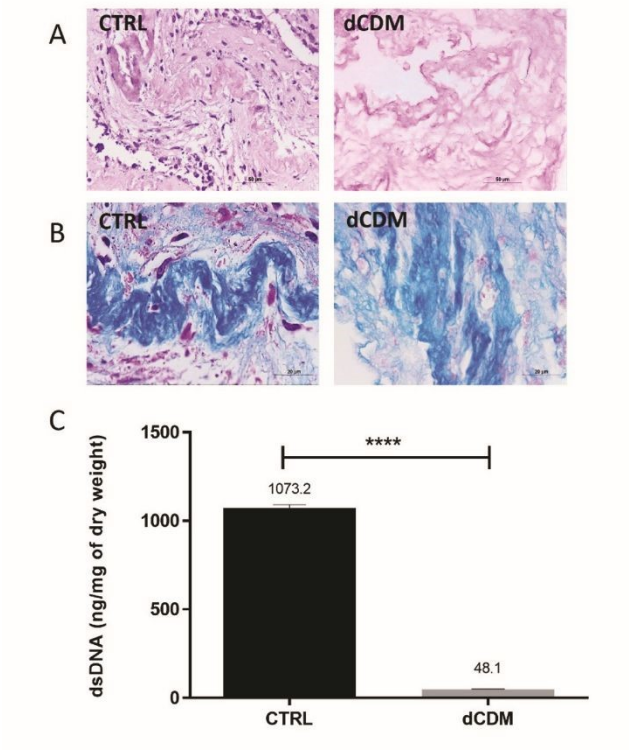

Figure 1 - **Characterization of decellularized material.** A) CTRL and dCDM stained with hematoxylin and eosin showing no nuclei present. B) Masson's Trichrome staining was performed on the CTRL and dCDM, evidencing the collagen content (scale bar: 50 µm). C) dsDNA quantification shows a significant decrease of dsDNA content on dCDM compared to CTRL, reaching less than 50 ng/mg of dCDM dry weight as postulated (****p≤0.0001).

Scaffold's structure evaluation

Scaffolds composed of SF, SF/dCDM, SF/CNT, and SF/dCDM/CNT were prepared and characterized using micro-CT, SEM, and DMA. The micro-CT and SEM were performed to analyze the porosity and structure of the scaffolds (Figure 2). The micro-CT analysis showed differences in pore size (Figure 2 A). As seen in Table 2, SF evidenced a mean pore size of 83 ± 9 µm, SF/dCDM a pore size of 135 ± 34 µm, SF/CNT and SF/dCDM/CNT a pore size of 63 ± 29 µm and 112 ± 22 µm, respectively. Additionally, the total porosity of SF was 73 ± 3%, of SF/dCDM was 76 ± 4%, and SF/CNT and SF/dCDM/CNT displayed a total porosity of 60 ± 3% and 75 ± 3%, respectively. SF/dCDM and SF/dCDM/CNT presented the highest total porosity and largest mean pore size. Images of scaffold structure obtained by micro-CT clearly show the different pore sizes (Figure 2 A), which corroborates the values obtained during quantitative analysis (Table 2). Nevertheless, it is essential to point out that no effect was observed in the scaffolds' size, all with ≈ 6 mm of diameter (Figure 2 A insets). Moreover, different densities of the various constituents of the scaffolds were observed, as depicted in Figure 2 B. In this sense, it is possible to detect the presence of dCDM (in blue) since it presents higher density than SF (in green), as well as the presence of CNT (in blue), being the formulation with dCDM and CNT the one with more differences in the density of the scaffold (Figure 2 B). Finally, SEM analysis evidenced the scaffolds' different porosities in accordance with the results obtained by micro-CT (Figure 2 C).

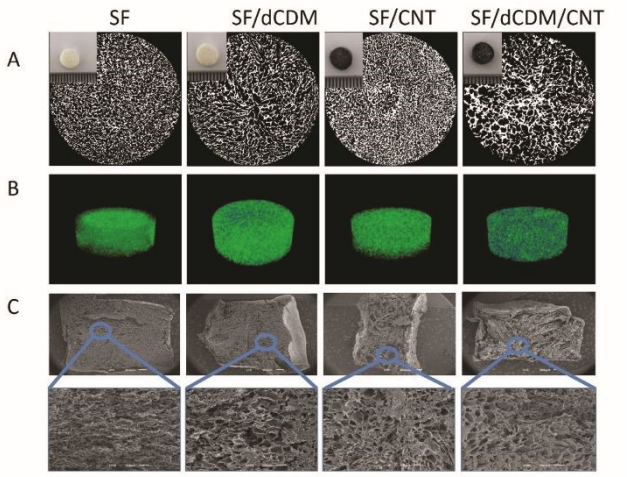

Figure 2 - Micro-CT and SEM analysis of SF, SF/dCDM, SF/CNT, and SF/dCDM/CNT scaffolds. (A) Micro-CT images showing scaffolds porosity. The inset shows pictures of the different scaffolds. (B) Visibility of different densities of the materials that form the scaffolds. (C) SEM images show the topography of scaffolds (scale bar:500 µm) and the respective porosity in higher magnification (scale bar:100 µm).

Table 2 - Micro-CT analysis results. Total porosity (%) and mean pore size (µm) for SF, SF/dCDM, SF/CNT, and SF/dCDM/CNT scaffolds.

Samples (n=3)	Total porosity (%)		Mean pore size (µm)	
	Mean	stdev	Mean	stdev
SF	73	3	83	9
SF/dCDM	76	4	135	34
SF/CNT	60	3	63	29
SF/dCDM/CNT	75	3	112	22

View Article Online
DOI: 10.1039/D1TB01972D

Furthermore, using micro-CT analysis, it was possible to assess the dispersion and possible aggregation of the CNT. For that, SF/dCDM scaffolds were used as a baseline, and the applied threshold was 25-255 for total content and 75/85-255 for differentiation of CNT. As depicted in Figure 3, it was possible to see low carbon nanotubes aggregation, thus indicating an adequate homogeneity in the scaffold matrix.

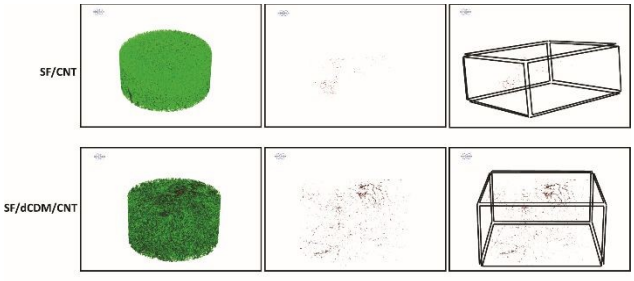

Figure 3 - Evaluation of carbon nanotube dispersion. Micro-CT analysis of SF/CNT and SF/dCDM/CNT showing nanotube aggregates (red regions) based on density, with SF/dCDM serving as the baseline.

DMA was performed to assess the mechanical properties of the scaffolds. The results showed that conditions containing dCDM (SF/dCDM and SF/dCDM/CNT scaffolds) possess approximately ten times lower E' (storage modulus, kPa) values as compared with SF and SF/CNT scaffolds (Figure 4 A). Tan δ (damping) was also analyzed, showing values below 1.0 that were constant up to 4 Hz for all conditions, evidencing that scaffolds' mechanical properties can be situated in the leathery region, meaning the scaffolds are rigid but flexible (Figure 4 B).

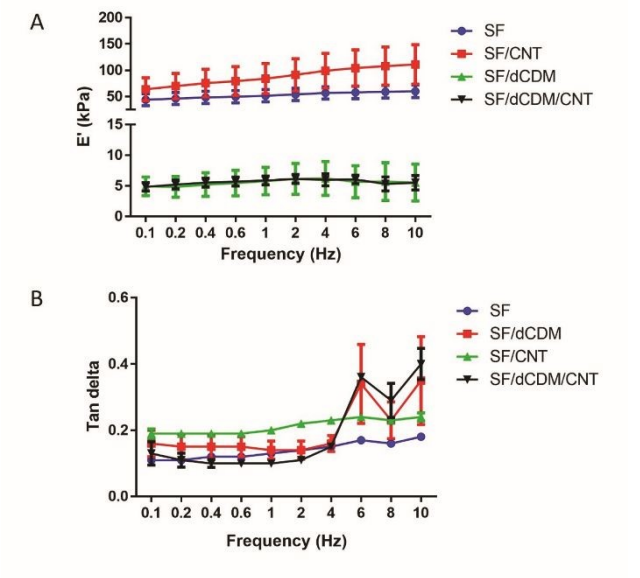

Figure 4 - DMA analysis. (A) Storage modulus (E'), and (B) Tan delta (Tanδ) of SF, SF/dCDM, SF/CNT, and SF/dCDM/CNT scaffolds measured as a function of frequency. Data are displayed as mean ± stdev (n=3).

In vitro bioactivity assessment

Bioactivity was investigated by soaking SF, SF/dCDM, SF/CNT, and SF/dCDM/CNT scaffolds in SBF at 37°C for 14 days. To evaluate mineralization formation, EDS was performed, and SEM images were obtained. For all conditions, mineralization was verified after 14 days, as depicted in Figure 5. Additionally, the formation of apatite crystals "cauliflower-like" structures on all samples were verified, except SF/CNT. The EDS analysis of SF/dCDM/CNT scaffolds showed higher amounts of calcium (Ca) and phosphorus (P) than SF/dCDM and SF/CNT scaffolds. When comparing SF scaffolds and SF/dCDM/CNT scaffolds, despite the

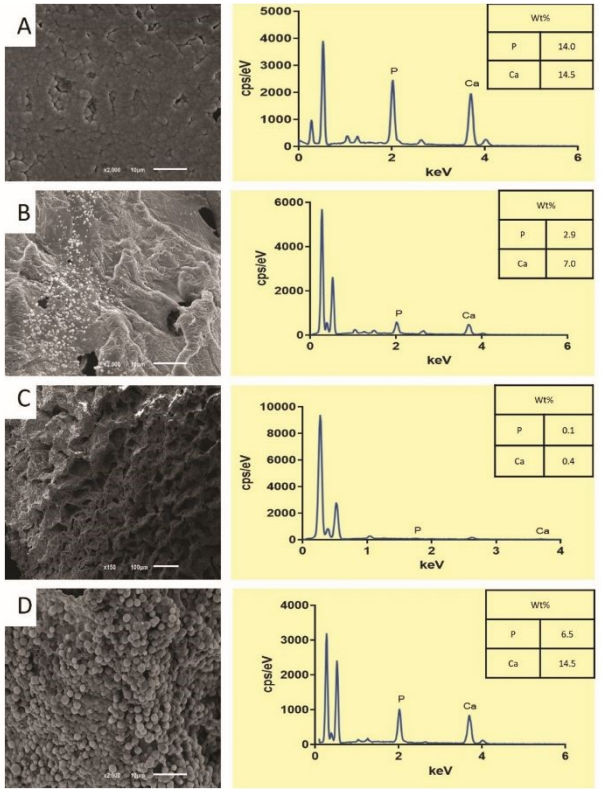

Figure 5 - In vitro bioactivity of SF, SF/dCDM, SF/CNT and SF/dCDM/CNT scaffolds. Representative SEM images and EDS analysis at day 14 of: (A) SF; (B) SF/dCDM; (C) SF/CNT; and (D) SF/dCDM/CNT scaffolds (scale bar: 10 µm).

similar values concerning the Ca content, it was observed lower values on P in SF/dCDM/CNT scaffolds.

Cellular *in vitro* studies

Metabolic activity

Metabolic activity was analyzed using Alamar Blue assay at 1, 14, and 21 days (Figure 6). The results were normalized using dsDNA quantification values. It was verified that the cells remained metabolic active after 21 days in each of the conditions. On day 1, cells cultured on SF/dCDM/CNT scaffolds

View Article Online
DOI: 10.1039/D1TB01972D

showed the highest metabolic activity among the four conditions. The cells cultured on SF/dCDM scaffolds showed the lowest metabolic activity. On day 14, the metabolic activity of cells cultured on SF/dCDM, SF/CNT, and SF/dCDM/CNT scaffolds decreased compared to day 1 while increasing for SF scaffolds. Nevertheless, cells cultured onto the SF/dCDM/CNT scaffolds also displayed the highest metabolic activity, and SF and SF/dCDM had the lowest values. Finally, on day 21, it was observed that the metabolic activity of cells cultured onto the SF/dCDM/CNT scaffolds decreased, but an increase in cells cultured onto the SF scaffolds was observed. When comparing day 14 and day 21, it was possible to watch a significant rise in metabolic activity values for SF, SF/dCDM, and SF/CNT cell-laden scaffolds. Moreover, the results showed that cells cultured onto SF/CNT scaffolds had significantly higher metabolic activity than the other three types of scaffolds at day 21.

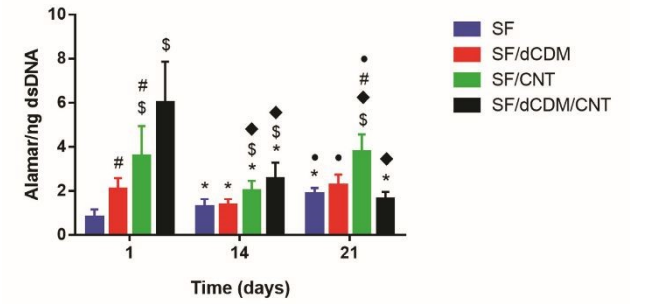

Figure 6 - Metabolic activity of cells seeded on scaffolds. Metabolic activity of hASCs seeded on SF, SF/dCDM, SF/CNT, and SF/dCDM/CNT scaffolds evaluated using Alamar Blue assay and normalized by ng of dsDNA. Data is displayed as mean±stdev (n=9). * - indicates statistically significant differences when compared with day 1; $ - indicates statistically significant differences when compared with SF at the same time-point; # - indicates statistically significant differences when compared with SF/dCDM/CNT at the same time-point; ♦ - indicates statistically significant differences when compared with SF/dCDM at the same time-point. • – indicates statistically significant differences between day 21 and day 14.

Cell Proliferation

Cell proliferation was also analyzed, as shown in Figure 7. For that, dsDNA was quantified at 1, 14, and 21 days of culture. On day 1, SF/dCDM constructs showed higher rates of cell proliferation than SF/CNT. On day 14, compared to day 1, a significant increase in cell proliferation was verified for all four conditions. Furthermore, SF/dCDM constructs displayed the highest amount of cell proliferation at this time point, while the lowest increase was demonstrated in the SF/CNT constructs. When analyzing the values of cell proliferation at day 21, it increased significantly in all conditions compared to day 1. Interestingly, when comparing day 21 and day 14, SF/CNT constructs displayed a significant increase in cell proliferation values. On day 21, it was verified that SF/dCDM/CNT samples presented higher cell proliferation than SF/dCDM and SF/CNT, but no statistical differences were observed compared with SF.

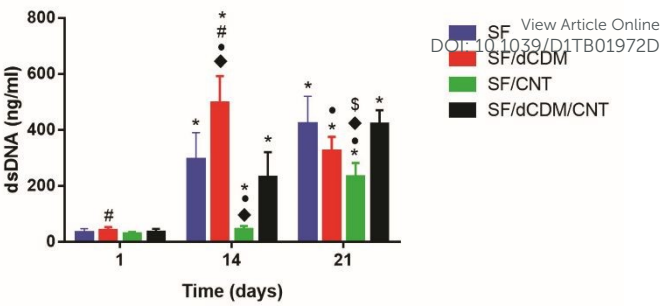

Figure 7 - Cell proliferation assessed by dsDNA quantification of hASCs seeded on SF, SF/dCDM, SF/CNT, and SF/dCDM/CNT. Data is displayed as mean±stdev (n=9). * - indicates statistically significant differences when compared with day 1; # - indicates statistical significant differences when compared with SF/CNT; • - indicates statistically significant differences when compared to SF/dCDM/CNT; ♦ - indicates statistically significant differences when compared with SF. $ - indicates statistically significant differences when compared to day 14.

Histology and SEM analysis

Histological analysis was performed on the seeded scaffolds after 21 days to assess the cell dispersion, morphology, and collagen production. Masson's Trichrome (TM) was performed to determine the collagen content on cell-seeded scaffolds. After 21 days, collagen was observed surrounding the cells for SF, SF/dCDM, and SF/dCDM/CNT, but no collagen was detected for SF/CNT conditions. Hematoxylin and eosin (HE) staining was used to observe cells grown on the scaffolds. The HE staining showed that after 21 days, cells were visible on the scaffold for all four conditions with some level of penetration into the scaffolds (Figure 8, black arrows).

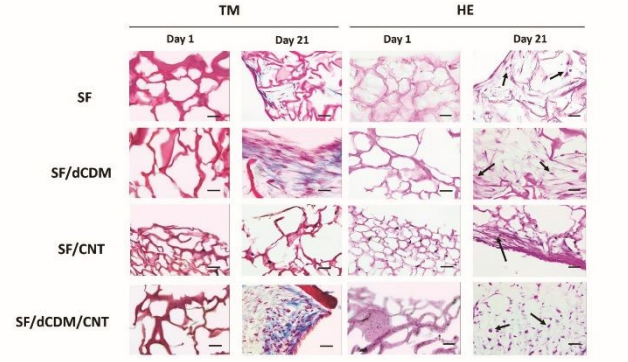

Figure 8 - Histological analysis. Representative images of Masson's Trichrome (TM) of hASCs cultured on SF, SF/dCDM, SF/CNT, and SF/dCDM/CNT scaffolds at day 1 and 21, staining collagen in blue (scale bar: 50 µm). Representative images of hematoxylin and eosin (HE) staining of hASCs cultured on SF, SF/dCDM, SF/CNT, and SF/dCDM/CNT scaffolds, on day 1, and 21 (scale bar:50 µm; black arrows indicate stained cells).

To further complement this data, SEM was performed after 21 days. It was possible to observe that the cells adhered and spread onto the different scaffolds, reaching a high degree of confluence. Furthermore, a good distribution of cells on the scaffold surface with some degree of penetration into the

matrix and consistent cell morphology was also observed

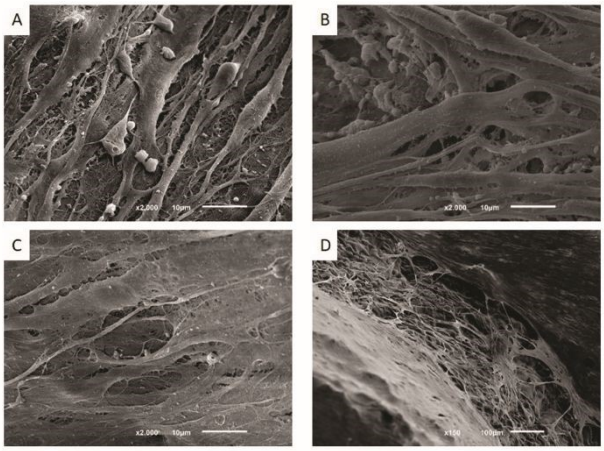

Figure 9 - SEM analysis. Visible cells are covering (A) SF scaffolds, (B) SF/dCDM scaffolds, (C) SF/CNT scaffolds, and (D) SF/dCDM/CNT scaffolds after 21 days of culture (scale bar: 10 µm).

(Figure 9).

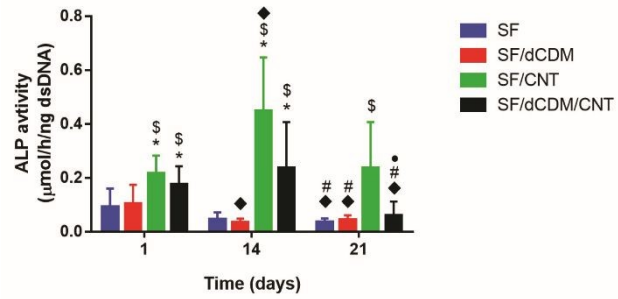

Figure 10 - Quantification of ALP activity of hASCs seeded onto the SF, SF/dCDM, SF/CNT, and SF/dCDM/CNT scaffolds for 21 days. Data is displayed as mean±stdev (n=9). * - indicates statistically significant differences when compared to SF; # - indicates statistic significant differences when compared to SF/CNT; $ - indicates statistically significant differences when compared to SF/dCDM; ♦ - indicates statistically significant differences when compared to day 1; • - indicates statistically significant differences when compared to day 14.

ALP activity quantification

ALP activity was quantified after 1, 14, and 21 days of culture and normalized by dsDNA (Figure 10). On day 1, SF and SF/dCDM constructs had significantly lower ALP expression than SF/CNT and SF/dCDM/CNT constructs. On day 14, compared to day 1, the values of ALP activity decreased for SF/dCDM constructs, while the values increased for SF/CNT constructs. Furthermore, similarly to day 1, SF samples had significantly lower ALP expression than SF/CNT and SF/dCDM/CNT, whereas SF/dCDM showed lower expression than SF/dCDM and SF/dCDM/CNT samples. On day 21, comparatively to day 1, an expression decreased was observed for SF, SF/dCDM, and SF/dCDM/CNT constructs. Also, comparatively to day 14, a decrease in ALP expression for SF/CNT and SF/dCDM/ CNT constructs was verified. Following the tendency of the previous time points, the expression of SF/CNT was higher than the other conditions.

PCR analysis

View Article Online
DOI: 10.1039/D1TB01972D

The differentiation of hASCs seeded onto the scaffolds was evaluated by quantifying the relative gene expression of osteogenic-associated markers Col Iα, Runx-2, OPN, and ALP (Figure 11). SF/CNT and SF/dCDM/CNT constructs expressed significantly higher levels of ALP than SF scaffolds at day 14. Moreover, at day 21, a significant decrease of ALP expression on SF/dCDM, SF/CNT, and SF/dCDM/CNT constructs was observed compared to day 14 (Figure 11 A). For Runx-2 gene expression, SF/CNT and SF/dCDM/CNT constructs showed significantly higher transcript levels than SF scaffolds at day 14. When comparing day 14 with day 21, a significant increase of Runx-2 expression was verified on SF constructs as opposed to the SF/dCDM/CNT constructs (Figure 11 B). The expression of Col Iα at day 14 was significantly higher in tested conditions as compared to control SF constructs. Moreover, the Col Iα transcript levels were significantly higher at day 14 compared to day 21. SF/dCDM/CNT constructs also showed at day 21 significantly higher Col Iα expression than that observed for SF and SF/dCDM constructs (Figure 11 C). Finally, the OPN transcript levels at day 14 were significantly higher on SF/CNT constructs than the other tested conditions. On day 21, a significant increase of OPN gene expression was verified on SF constructs, which together with SF/CNT constructs showed significantly higher OPN transcript levels than that observed on SF/dCDM and SF/dCDM/CNT constructs at the same culture period (Figure 11 D).

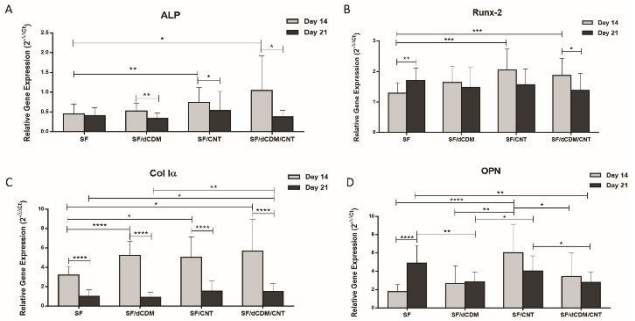

Figure 11 - Real-time qRT-PCR analysis for different osteogenic associated genes. Relative expression of osteogenic-related transcripts, namely (A) ALP, (B) Runx-2, (C) Col Iα, and (D) OPN, by the hASCs cultured on SF, SF/dCDM, SF/CNT, and SF/dCDM/CNT scaffolds for 14 and 21 days. The 2−ΔΔCt method was used to calculate the fold changes in relative gene expression. The significance levels were set to p≤0.05 (*), p≤0.01 (**), p≤0.001 (***), and p≤0.0001 (****).

Cell viability and morphology

After 1, 14, and 21 days of culture, the cell viability and morphology were evaluated under a fluorescence microscope (Figure 12). A live/dead assay was performed to assess cell viability, staining live cells in green and dead cells in red. For all conditions, cells remained viable along the time of culture, as depicted in Figure 12. After 21 days, a high number of viable cells was seen, contrasting with the low number of dead cells. Additionally, it was possible to observe that cells proliferated

along the 21 days. To assess the morphology of cells, the cytoskeleton was stained using Phalloidin (in red), and the nucleus was stained with DAPI (in blue). As observed from Figure 12, the cells presented a round shape after 1 day of culture, but they shifted to a spindle-like form along with the

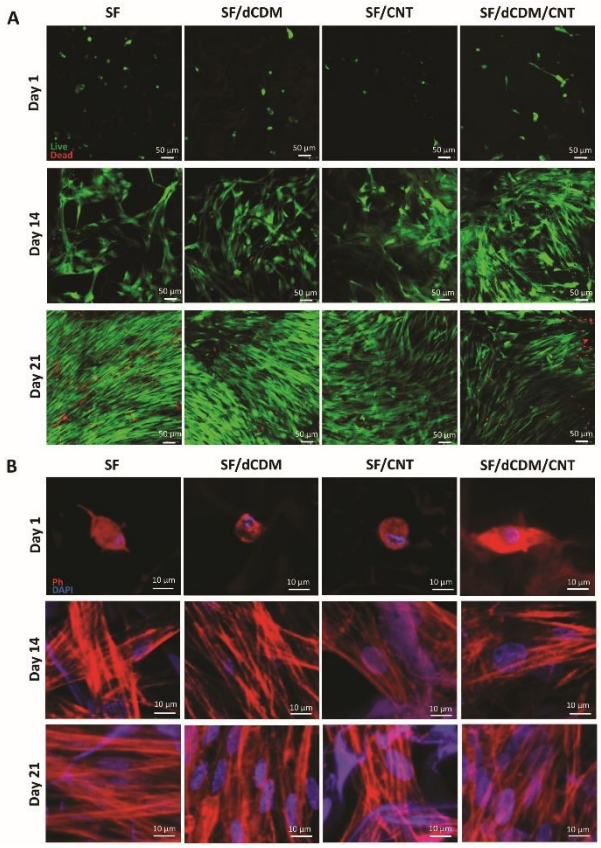

Figure 12 - Cell viability and morphology. Representative images of viability and morphology of hASCs cultured on SF scaffolds, SF/, SF/CNT scaffolds, and SF/dCDM/CNT scaffolds through 21 days. (A) Live/dead imaging showing viable cells stained in green and dead cells stained in red (scale bar: 50 µm), (B) Pictures show cells' cytoskeleton and nucleus upon stained with Phalloidin (in red) and DAPI (in blue), respectively (scale bar: 10 µm).

culture for all conditions.

Scaffolds hemocompatibility

A hemolytic assay was performed to assess the hemocompatibility of the scaffolds. For all four different scaffolds formulations, the obtained value of hemolysis percentage was 0%, indicating no bursts of blood cells (Figure 13).

View Article Online
DOI: 10.1039/D1TB01972D

Figure 13 - Results of hemolytic assay. Results of the hemolytic assay on SF, SF/dCDM, SF/CNT, and SF/dCDM/CNT scaffolds with PBS acting as a negative control group (CTRL -) and Triton X-100 as a positive control group (CTRL+).

Samples	Hemolysis (%)	
SF	0	
SF/dCDM	0	
SF/CNT	0	
SF/dCDM/CNT	0	
CTRL$^-$	0	
CTRL$^+$	100	

Discussion

Currently, in bone tissue engineering (BTE), the natural step forward is developing biomimetic approaches that recapitulate the native tissues environment, ideal for regeneration of bone tissue.[22] The existent scaffold approaches do not yet possess the specificity to mimic the different dimensions of the natural tissue. Hence, the challenge remains the development of more efficient hierarchical scaffolds.

SF was combined with dCDM and CNT in the present study to produce carbon nanotubes-reinforced cell-derived matrix-silk fibroin hierarchical scaffolds to mimic the bone structure from macro to nanoscale. These scaffolds were evaluated regarding their mechanical and structural properties and their effects on cells behavior, namely viability, proliferation, and differentiation along the osteoblastic lineage. Firstly, the efficient decellularization of the dCDM was verified using hematoxylin and eosin staining to guarantee the absence of visible nuclei. This verification is of great importance since it prevents an immunological response and is critical for further application of the dCDM.[23] Furthermore, Masson's Trichrome showed apparent preservation of collagen in the dCDM. Several studies have reported the importance of collagen on cellular differentiation since it contains several biological cues that can modulate cells adhesion, proliferation, and differentiation.[24] DNA quantification was also performed, demonstrating that the dsDNA content was below 50 ng/mg of matrix dry weight, the accepted threshold for effective decellularization.[21]

Another vital aspect of hierarchical scaffold production is its mechanical and structural properties. A minimum pore size ranging from 100 µm to 150 µm has been described as required for bone formation.[25] Also, scaffolds should ideally possess

View Article Online
DOI: 10.1039/D1TB01972D

between 60% - 90% of total porosity.[26] The scaffold's porosity analysis showed that CNT appears to have a decreasing effect on pore size since the SF/CNT scaffolds presented the lowest pore size (63 ± 29 µm) and total porosity (60 ± 3%). On the other hand, the incorporation of dCDM seems to increase the pore size since SF/dCDM and SF/dCDM/CNT present a pore size of 135 ± 34 µm and 112 ± 22 µm, respectively, countering the previously described effect of the CNT. The pore size observed was smaller than verified by Ribeiro *et al*., who used SF and HRP/H_2O_2 to fabricate scaffolds using enzymatic cross-linking and salt leaching. They observed a mean pore size of 361.4 µm.[27] This pore size indicates that the chosen processing method can drastically influence pore size. The one selected for this work successfully resulted in pores sizes within the described optimum range for bone formation. In a similar manner to pore size, total porosity increased with the presence of dCDM, to 76 ± 4% in the case of SF/dCDM and 75 ± 3% in the case of SF/CNT/dCDM. The results are also within the optimum range and around 10 % superior, as reported by Costa *et al*. that observed a 59.1% total porosity for the SF scaffold.[28] Besides these observations, micro-CT results also showed that CNT appears to be adequately dispersed through the scaffolds matrix. This observation is crucial since CNT are predisposed to entangle and form agglomerates due to van der Waals forces between the tubes, and such accumulation may hinder its application.[29]

Considering the mechanical analysis, although the positive effect on pore size, the conditions modified with dCDM showed a much ten times lower storage modulus than SF and SF/CNT scaffolds. The weaker mechanical properties can be explained by the presence of collagen in the dCDM, as verified by Masson's Trichrome, which is widely known to present low storage modulus.[30,31] Furthermore, all scaffolds were elastic, as evidenced by the tan δ (<1) values. Results showed that even though the porosity of the conditions modified with dCDM is more suitable for bone regeneration, its incorporation also results in much weaker mechanical properties. Such mechanical properties are very different from native bone tissue stiffness (e.g., ≈ 20 GPa in the case of cortical bone).[31] Interestingly, studies have shown that scaffolds with lower stiffness (< 0.7 kPa) were capable of stimulating cell proliferation and osteogenic differentiation at a higher level than stiffer scaffolds (> 5 kPa).[32,33] Thus, the scaffolds with dCDM are within the limit of the optimum scaffolds' stiffness values to promote the differentiation along the osteogenic lineage. Interestingly, although the mechanical properties enhancing effect of CNT is well documented [34], the obtained data showed no effect of CNT on the improvement of stiffness. The low concentration of CNT used for the scaffold production could explain these results. Besides, scaffolds were soaked in SBF solution to evaluate its bioactivity and thus foresee its behavior upon implanted in an *in vivo* environment. SF scaffolds showed to be bioactive as expected since silk bioactivity is well known and widely studied.[35] The results of SF/dCDM/CNT scaffolds showed a very similar apatite deposition to that observed for the SF scaffolds, thus suggesting that the addition of dCDM and CNT negatively affected the bioactive behavior of scaffolds.

The effect of the developed scaffolds on cells was studied using hASCs cultured without supplemented medium, namely in terms of cell adhesion and spreading, metabolic activity, cell proliferation, ALP activity, and gene expression. Cells seeded on SF, SF/dCDM, and SF/CNT scaffolds evidenced an increase in metabolic activity across all time points, in opposition to SF/dCDM/CNT constructs where the metabolic activity decreased from day 1 to day 14. Additionally, for SF/dCDM/CNT, between day 14 and day 21, the stagnation of metabolic activity is consistent with the stagnated cell proliferation, which indicates that cells were beginning to differentiate along the osteoblastic lineage. It is widely accepted that when cells began to differentiate, they became less proliferative, as observed between day 14 and day 21.[36] Interestingly, between day 1 and day 14, SF/dCDM evidencing the highest cell proliferation rate, which could be related to the presence of dCDM. It is described in the literature that scaffolds with cell-derived matrices present improved cell proliferation rates.[37,38] Moreover, the lower stiffness of the scaffolds can result as well in improved cell proliferation.[32] SEM images showed that the scaffolds were covered entirely in cells with a high degree of confluence, corroborating that the cells were proliferating along the time of culture. This was further evidenced by Phalloidin-DAPI images, where cell elongation and random cell orientation could be seen. Additionally, the live-dead analysis showed that scaffolds had no harmful effects on cells across the 21 days of culture. According to the previous results, HE staining also evidenced cell adhesion and spread across the surface with penetration into the scaffold interior. Furthermore, Masson's Trichrome showed the presence of *de novo* collagen in all conditions except SF/CNT, indicating that cells were capable of producing and secreting their endogenous collagenous matrix at their pericellular space. These results suggest that CNT by itself may have a negative effect on collagen production, which can be countered by the presence of dCDM. In fact, in conditions containing dCDM, cells could express collagen even in the presence of CNT. This observation contradicts the predominant trend on CNT effects on collagen production described in the literature since multiple studies have found that CNT positively impacts collagen production.[39,40] Considering this observation, further analysis will be necessary to comprehend this result better.

Regarding the evaluation of osteogenic differentiation, ALP, an early marker for osteogenic differentiation and ordinarily present in high concentrations in growing bone, was assessed.[41] ALP activity of cells seeded on SF/CNT and SF/dCDM/CNT scaffolds expressed the typical peak activity on day 14 with the subsequent decrease, as expected, suggesting that cells were differentiating along the osteoblastic lineage.[42] Furthermore, it is well known and accepted that a reduction in ALP expression is associated with differentiation and mineralization.[42] In this reasoning, the higher ALP activity observed on cells seeded on SF/CNT and SF/dCDM/CNT scaffolds might suggest more significant osteogenic potential. Similar results have been found in previous studies showing enhanced ALP activity in carbon nanotubes-modified scaffolds.[43] It is noteworthy that although dCDM had a visibly

View Article Online
DOI: 10.1039/D1TB01975D

positive effect on cell proliferation, the same was not verified for ALP activity. This result was not expected since the evidence found in the literature indicates that cell-derived matrices positively affect the ALP activity.[37] For so, further investigation will be needed to clarify such results.

Different osteogenic markers were assessed regarding gene expression levels, namely ALP, Runx-2, OPN, and Col Iα. As expected, the early osteogenic differentiation markers, ALP and Runx-2, were expressed at day 14, decreasing at day 21.[44,45] Consistent with ALP activity results, the increased gene expression profile of ALP and Runx-2 on SF/CNT and SF/dCDM/CNT suggests that the addition of CNT stimulates osteogenic cell differentiation. According to these results, other studies have found that the use of CNT upregulates Runx-2 (46) and ALP (47) gene expression. In the case of OPN, important in bone modeling (48) and collagen production (49), SF/CNT and SF/dCDM/CNT are the only conditions that displayed an early expression pattern for both markers. Furthermore, on day 14, SF/CNT showed higher OPN expression than SF/dCDM/CNT, thus suggesting that cells cultured on SF/dCDM/CNT scaffolds were further advanced in the differentiation stage. Additionally, upregulation of OPN expression on conditions with CNT was also observed.[46] For Col Iα, an osteogenic differentiation marker related to bone formation and bone architecture (50), the results showed higher expression on SF/dCDM, SF/CNT, and SF/dCDM/CNT than on pure SF constructs. This result suggests that the osteogenic potential of these scaffolds is superior as compared to the control. It is essential to highlight that SF/CNT and SF/dCDM/CNT constructs presented a significant up-regulation of all four tested genes comparatively to the pure SF scaffolds, evidencing the proposed composite materials as promoters of osteogenic differentiation.

Finally, the hemolytic assay was performed to evaluate hemoglobin release in the plasma (indication of red blood cell lysis) on all conditions. According to Testing and Materials, a material is considered safe when its hemolysis percentage is under 2%, while a 5% limit is specified by ISO 10 993-5.[51,52] Results showed no hemolytic effect for any of the scaffolds. Hence, the findings show that the scaffolds are hemocompatible, making them suitable for further in vivo applications.

Conclusions

In this study, novel 3D silk fibroin hierarchical scaffolds were produced and evaluated according to their mechanical, structural, and biological properties for bone applications. The results showed that the combination of CNT and dCDM affected the SF scaffold's structure and mechanical properties. In this sense, its combination resulted in the development of an elastic and bioactive scaffold with pore sizes (≈ 112 ± 22 μm), total porosity (75 ± 3%), and stiffness's (≈ 5 kPa) within the range described for the stimulation of cell's differentiation along the osteogenic lineage. Furthermore, carbon nanotubes-reinforced cell-derived matrix-silk fibroin hierarchical scaffolds showed to support cells' adhesion, spreading, proliferation, and ultimately, osteogenic differentiation, as demonstrated by the secretion of collagen, the increase of ALP activity, and the increase of osteogenic related genes' expression, namely, ALP, Runx-2, Col Iα and OPN comparing to SF scaffolds. Overall, the developed carbon nanotubes-reinforced cell-derived matrix-silk fibroin hierarchical scaffolds showed great potential for applications in bone tissue engineering.

.

Conflicts of interest

There are no conflicts to declare.

Acknowledgments

The authors thank the funds provided by the Research and Innovation Staff Exchanges (RISE) action (H2020 Marie Skłodowska-Curie actions) for funds obtained through the BAMOS project (H2020-MSCA-RISE-2016-73415) and the R&D Project KOAT PTDC/BTMMAT/29760/2017 (POCI-01-0145-FEDER-029760), financed by Fundação para a Ciência e a Tecnologia (FCT) and co-financed by FEDER and POCI. F.R.M. acknowledges FCT for her contract under the Transitional Rule DL 57/2016 (CTTI-57/18-I3BS(5)). V.P.R. acknowledges the Junior Researcher contracts (POCI-01-0145-FEDER-031367; POCI-01-0145-FEDER-029139) attributed by the FCT under the projects Fun4TE project (PTDC/EMD-EMD/31367/2017) and B-Liver (PTDC/EMD-EMD/29139/2017). J.B.C. acknowledges the Junior Researcher contract (POCI-01-0145-FEDER-031367) attributed by FCT to the Fun4TE project (PTDC/EMD-EMD/31367/2017).

Notes and references

1 Agarwal R, García AJ. Biomaterial strategies for engineering implants for enhanced osseointegration and bone repair. Adv Drug Deliv Rev. 2015 Nov;94:53–62.
2 Amini Z, Lari R. A systematic review of decellularized allograft and xenograft-derived scaffolds in bone tissue regeneration. Tissue Cell. 2021 Apr;69:101494.
3 Roseti L, Parisi V, Petretta M, Cavallo C, Desando G, Bartolotti I, et al. Scaffolds for Bone Tissue Engineering: State of the art and new perspectives. Mater Sci Eng C Mater Biol Appl. 2017 Sep;78:1246–62.
4 Li JJ, Ebied M, Xu J, Zreiqat H. Current Approaches to Bone Tissue Engineering: The Interface between Biology and Engineering. Adv Healthc Mater [Internet]. 2018 Mar 1;7(6):1701061. Available from: https://doi.org/10.1002/adhm.201701061
5 Canadas RF, Ren T, Marques AP, Oliveira JM, Reis RL, Demirci U. Biochemical Gradients to Generate 3D Heterotypic-Like Tissues with Isotropic and Anisotropic Architectures. Adv Funct Mater [Internet]. 2018 Nov 1;28(48):1804148. Available from: https://doi.org/10.1002/adfm.201804148
6 Murahashi Y, Yano F, Nakamoto H, Maenohara Y, Iba K, Yamashita T, et al. Multi-layered PLLA-nanosheets loaded with FGF-2 induce robust bone regeneration with controlled release in critical-sized mouse femoral defects. Acta Biomater [Internet]. 2019;85:172–9. Available from: http://www.sciencedirect.com/science/article/pii/S1742706118307566

7 Kim HD, Amirthalingam S, Kim SL, Lee SS, Rangasamy J, Hwang NS. Biomimetic Materials and Fabrication Approaches for Bone Tissue Engineering. Adv Healthc Mater [Internet]. 2017 Dec 1;6(23):1700612. Available from: https://doi.org/10.1002/adhm.201700612

8 Wen J, Yao J, Chen X, Shao Z. Silk Fibroin Acts as a Self-Emulsifier to Prepare Hierarchically Porous Silk Fibroin Scaffolds through Emulsion-Ice Dual Templates. ACS omega. 2018 Mar;3(3):3396–405.

9 Bhattacharjee P, Kundu B, Naskar D, Kim H-W, Maiti TK, Bhattacharya D, et al. Silk scaffolds in bone tissue engineering: An overview. Acta Biomater. 2017 Nov;63:1–17.

10 Liu B, Gao X, Sun Z, Fang Q, Geng X, Zhang H, et al. Biomimetic porous silk fibroin/biphasic calcium phosphate scaffold for bone tissue regeneration. J Mater Sci Mater Med. 2018 Dec;30(1):4.

11 Ou L, Lan Y, Feng Z, Feng L, Yang J, Liu Y, et al. Functionalization of SF/HAP Scaffold with GO-PEI-miRNA inhibitor Complexes to Enhance Bone Regeneration through Activating Transcription Factor 4. Theranostics. 2019;9(15):4525–41.

12 Melke J, Midha S, Ghosh S, Ito K, Hofmann S. Silk fibroin as biomaterial for bone tissue engineering. Acta Biomater [Internet]. 2016;31:1–16. Available from: http://www.sciencedirect.com/science/article/pii/S1742706115300982

13 Ding Z, Cheng W, Mia MS, Lu Q. Silk Biomaterials for Bone Tissue Engineering. Macromol Biosci. 2021 Jun;e2100153.

14 Gonçalves EM, Oliveira FJ, Silva RF, Neto MA, Fernandes MH, Amaral M, et al. Three-dimensional printed PCL-hydroxyapatite scaffolds filled with CNTs for bone cell growth stimulation. J Biomed Mater Res B Appl Biomater. 2016 Aug;104(6):1210–9.

15 Liu L, Yang B, Wang L-Q, Huang J-P, Chen W-Y, Ban Q, et al. Biomimetic bone tissue engineering hydrogel scaffolds constructed using ordered CNTs and HA induce the proliferation and differentiation of BMSCs. J Mater Chem B. 2020 Jan;8(3):558–67.

16 Han L, Sun H, Tang P, Li P, Xie C, Wang M, et al. Mussel-inspired graphene oxide nanosheet-enwrapped Ti scaffolds with drug-encapsulated gelatin microspheres for bone regeneration. Biomater Sci. 2018 Feb;6(3):538–49.

17 Szymański T, Mieloch AA, Richter M, Trzeciak T, Florek E, Rybka JD, et al. Utilization of Carbon Nanotubes in Manufacturing of 3D Cartilage and Bone Scaffolds. Mater (Basel, Switzerland) [Internet]. 2020 Sep 11;13(18):4039. Available from: https://pubmed.ncbi.nlm.nih.gov/32933020

18 Alom N, Peto H, Kirkham GR, Shakesheff KM, White LJ. Bone extracellular matrix hydrogel enhances osteogenic differentiation of C2C12 myoblasts and mouse primary calvarial cells. J Biomed Mater Res Part B Appl Biomater [Internet]. 2018 Feb 1;106(2):900–8. Available from: https://doi.org/10.1002/jbm.b.33894

19 Maia FR, Reis RL, Oliveira JM. Decellularized hASCs-derived matrices as biomaterials for 3D in vitro approaches. Methods Cell Biol. 2020;156:45–58.

20 Cüneyt Tas A. Synthesis of biomimetic Ca-hydroxyapatite powders at 37°C in synthetic body fluids. Biomaterials [Internet]. 2000;21(14):1429–38. Available from: https://www.sciencedirect.com/science/article/pii/S0142961200000193

21 Crapo PM, Gilbert TW, Badylak SF. An overview of tissue and whole organ decellularization processes. Biomaterials [Internet]. 2011;32(12):3233–43. Available from: http://dx.doi.org/10.1016/j.biomaterials.2011.01.057

22 Du Y, Guo JL, Wang J, Mikos AG, Zhang S. Hierarchically designed bone scaffolds: From internal cues to external stimuli. Biomaterials [Internet]. 2019/07/03. 2019 Oct;218:119334. Available from: https://pubmed.ncbi.nlm.nih.gov/31306826

23 Choudhury D, Yee M, Sheng ZLJ, Amirul A, Naing MW. Decellularization systems and devices: State-of-the-art. Acta Biomater [Internet]. 2020;115:51–9. Available from: https://www.sciencedirect.com/science/article/pii/S1742706120304580X

24 Rico-Llanos GA, Borrego-González S, Moncayo-Donoso M, Becerra J, Visser R. Collagen Type I Biomaterials as Scaffolds for Bone Tissue Engineering. Polymers (Basel) [Internet]. 2021 Feb 17;13(4):599. Available from: https://pubmed.ncbi.nlm.nih.gov/33671329

25 Bose S, Vahabzadeh S, Bandyopadhyay A. Bone tissue engineering using 3D printing. Mater Today [Internet]. 2013;16(12):496–504. Available from: https://www.sciencedirect.com/science/article/pii/S1369702113004010X

26 Marew T, Birhanu G. Three dimensional printed nanostructure biomaterials for bone tissue engineering. Regen Ther [Internet]. 2021 May 28;18:102–11. Available from: https://pubmed.ncbi.nlm.nih.gov/34141834

27 Ribeiro VP, da Silva Morais A, Maia FR, Canadas RF, Costa JB, Oliveira AL, et al. Combinatory approach for developing silk fibroin scaffolds for cartilage regeneration. Acta Biomater [Internet]. 2018;72:167–81. Available from: https://www.sciencedirect.com/science/article/pii/S1742706118301788

28 Costa JB, Silva-Correia J, Oliveira JM, Reis RL. Fast Setting Silk Fibroin Bioink for Bioprinting of Patient-Specific Memory-Shape Implants. Adv Healthc Mater [Internet]. 2017 Nov 1;6(22):1701021. Available from: https://doi.org/10.1002/adhm.201701021

29 Liang C, Wang B, Chen J, Yong Q, Huang Y, Liao B. Dispersion of Multi-Walled Carbon Nanotubes by Polymers with Carbazole Pendants. J Phys Chem B [Internet]. 2017 Sep 7;121(35):8408–16. Available from: https://doi.org/10.1021/acs.jpcb.7b05481

30 Wu C-C, Ding S-J, Wang Y-H, Tang M-J, Chang H-C. Mechanical properties of collagen gels derived from rats of different ages. J Biomater Sci Polym Ed. 2005;16(10):1261–75.

31 Guimarães CF, Gasperini L, Marques AP, Reis RL. The stiffness of living tissues and its implications for tissue engineering. Nat Rev Mater [Internet]. 2020;5(5):351–70. Available from: https://doi.org/10.1038/s41578-019-0169-1

32 Zhang J, Wehrle E, Adamek P, Paul GR, Qin X-H, Rubert M, et al. Optimization of mechanical stiffness and cell density of 3D bioprinted cell-laden scaffolds improves extracellular matrix mineralization and cellular organization for bone tissue engineering. Acta Biomater [Internet]. 2020;114:307–22. Available from: https://www.sciencedirect.com/science/article/pii/S1742706120304013

33 Maia FR, Fonseca KB, Rodrigues G, Granja PL, Barrias CC. Matrix-driven formation of mesenchymal stem cell-extracellular matrix microtissues on soft alginate hydrogels. Acta Biomater. 2014 Jul;10(7):3197–208.

34 Peng Z, Zhao T, Zhou Y, Li S, Li J, Leblanc RM. Bone Tissue Engineering via Carbon-Based Nanomaterials. Adv Healthc Mater [Internet]. 2020 Mar 1;9(5):1901495. Available from: https://doi.org/10.1002/adhm.201901495

35 Zhang H, You R, Yan K, Lu Z, Fan Q, Li X, et al. Silk as templates for hydroxyapatite biomineralization: A comparative study of Bombyx mori and Antheraea pernyi silkworm silks. Int J Biol Macromol. 2020 Dec;164:2842–50.

36 Ruijtenberg S, van den Heuvel S. Coordinating cell proliferation and differentiation: Antagonism between cell cycle regulators and cell type-specific gene expression. Cell Cycle. 2016;15(2):196–212.

37 Kim IG, Hwang MP, Du P, Ko J, Ha C, Do SH, et al. Bioactive cell-derived matrices combined with polymer mesh scaffold for osteogenesis and bone healing. Biomaterials. 2015 May;50:75–86.
38 Assunção M, Dehghan-Baniani D, Yiu CHK, Später T, Beyer S, Blocki A. Cell-Derived Extracellular Matrix for Tissue Engineering and Regenerative Medicine. Front Bioeng Biotechnol. 2020;8:602009.
39 Sá MA, Ribeiro HJ, Valverde TM, Sousa BR, Martins-Júnior PA, Mendes RM, et al. Single-walled carbon nanotubes functionalized with sodium hyaluronate enhance bone mineralization. Brazilian J Med Biol Res = Rev Bras Pesqui medicas e Biol [Internet]. 2015/12/04. 2016 Feb;49(2):e4888–e4888. Available from: https://pubmed.ncbi.nlm.nih.gov/26648087
40 Andrade VB, Sá MA, Mendes RM, Martins-Júnior PA, Silva GAB, Sousa BR, et al. Enhancement of Bone Healing by Local Administration of Carbon Nanotubes Functionalized with Sodium Hyaluronate in Rat Tibiae. Cells Tissues Organs. 2017;204(3–4):137–49.
41 Zhou T, Chen S, Ding X, Hu Z, Cen L, Zhang X. Fabrication and Characterization of Collagen/PVA Dual-Layer Membranes for Periodontal Bone Regeneration. Front Bioeng Biotechnol. 2021;9:630977.
42 Jaiswal N, Haynesworth SE, Caplan AI, Bruder SP. Osteogenic differentiation of purified, culture-expanded human mesenchymal stem cells in vitro. J Cell Biochem. 1997 Feb;64(2):295–312.
43 Pan L, Pei X, He R, Wan Q, Wang J. Multiwall carbon nanotubes/polycaprolactone composites for bone tissue engineering application. Colloids Surfaces B Biointerfaces [Internet]. 2012;93:226–34. Available from: https://www.sciencedirect.com/science/article/pii/S0927776512000367
44 Yong KW, Choi JR, Choi JY, Cowie AC. Recent Advances in Mechanically Loaded Human Mesenchymal Stem Cells for Bone Tissue Engineering. Int J Mol Sci [Internet]. 2020 Aug 13;21(16):5816. Available from: https://pubmed.ncbi.nlm.nih.gov/32823645
45 Radwan-Pragłowska J, Janus Ł, Piątkowski M, Bogdał D, Matysek D. 3D Hierarchical, Nanostructured Chitosan/PLA/HA Scaffolds Doped with TiO(2)/Au/Pt NPs with Tunable Properties for Guided Bone Tissue Engineering. Polymers (Basel). 2020 Apr;12(4).
46 Liu X, George MN, Park S, Miller Ii AL, Gaihre B, Li L, et al. 3D-printed scaffolds with carbon nanotubes for bone tissue engineering: Fast and homogeneous one-step functionalization. Acta Biomater. 2020 Jul;111:129–40.
47 Li X, Liu H, Niu X, Yu B, Fan Y, Feng Q, et al. The use of carbon nanotubes to induce osteogenic differentiation of human adipose-derived MSCs in vitro and ectopic bone formation in vivo. Biomaterials. 2012 Jun;33(19):4818–27.
48 Bonventre J V, Sabbisetti V. Chapter 48 - Acute Kidney Injury: Biomarkers from Bench to Bedside. In: Himmelfarb J, Sayegh Dialysis, and Transplantation (Third Edition) MHBT-CKD, editors. Philadelphia: W.B. Saunders; 2010. p. 668–76. Available from: https://www.sciencedirect.com/science/article/pii/B9781437709872000480
49 Marra F, Caligiuri A. Chapter 5 - Cytokine Production and Signaling in Stellate Cells. In: Gandhi CR, Pinzani MBT-SC in H and D, editors. Boston: Academic Press; 2015. p. 63–86. Available from: https://www.sciencedirect.com/science/article/pii/B9780128001349000051
50 Hayrapetyan A, Bongio M, Leeuwenburgh SCG, Jansen JA, van den Beucken JJJP. Effect of Nano-HA/Collagen Composite Hydrogels on Osteogenic Behavior of Mesenchymal Stromal Cells. Stem cell Rev reports. 2016 Jun;12(3):352–64.
51 Weber M, Steinle H, Golombek S, Hann L, Schlensak C, Wendel HP, et al. Blood-Contacting Biomaterials: In Vitro Evaluation of the Hemocompatibility. Front Bioeng Biotechnol. 2018;6:99.
52 Zhou HY, Zhang YP, Zhang WF, Chen XG. Biocompatibility and characteristics of injectable chitosan-based thermosensitive hydrogel for drug delivery. Carbohydr Polym [Internet]. 2011;83(4):1643–51. Available from: https://www.sciencedirect.com/science/article/pii/S0144861710008283

View Article Online
DOI: 10.1039/D1TB01972D